Quantum-state-resolved reactivity of overtone excited CH_4 on Ni(111): Comparing experiment and theory

P. Morten Hundt, Maarten E. van Reijzen, Rainer D. Beck, Han Guo, and Bret Jackson

Citation: J. Chem. Phys. **146**, 054701 (2017); doi: 10.1063/1.4975025
View online: http://dx.doi.org/10.1063/1.4975025
View Table of Contents: http://aip.scitation.org/toc/jcp/146/5
Published by the American Institute of Physics

Quantum-state-resolved reactivity of overtone excited CH_4 on Ni(111): Comparing experiment and theory

P. Morten Hundt,[1] Maarten E. van Reijzen,[1] Rainer D. Beck,[1] Han Guo,[2] and Bret Jackson[2]
[1]*Laboratoire de Chimie Physique Moléculaire, Ecole Polytechnique Fédérale de Lausanne, 1015 Lausanne, Switzerland*
[2]*Department of Chemistry, University of Massachusetts, Amherst, Massachusetts 01003, USA*

(Received 18 November 2016; accepted 16 January 2017; published online 1 February 2017)

Quantum state resolved reactivity measurements probe the role of vibrational symmetry on the vibrational activation of the dissociative chemisorption of CH_4 on Ni(111). IR-IR double resonance excitation in a molecular beam was used to prepare CH_4 in three different vibrational symmetry components, A_1, E, and F_2, of the $2\nu_3$ antisymmetric stretch overtone vibration as well as in the $\nu_1 + \nu_3$ symmetric plus antisymmetric C–H stretch combination band of F_2 symmetry. The quantum state specific dissociation probability S_0 (sticking coefficient) was measured for each of the four vibrational states by detecting chemisorbed carbon on Ni(111) as the product of CH_4 dissociation by Auger electron spectroscopy. We observe strong mode specificity, where S_0 for the most reactive state $\nu_1 + \nu_3$ is an order of magnitude higher than for the least reactive, more energetic $2\nu_3$-E state. Our first principles quantum scattering calculations show that as molecules in the ν_1 state approach the surface, the vibrational amplitude becomes localized on the reacting C–H bond, making them very reactive. This behavior results from the weakening of the reacting C–H bond as the molecule approaches the surface, decoupling its motion from the three non-reacting C–H stretches. Similarly, we find that overtone normal mode states with more ν_1 character are more reactive: $S_0(2\nu_1) > S_0(\nu_1 + \nu_3) > S_0(2\nu_3)$. The $2\nu_3$ eigenstates excited in the experiment can be written as linear combinations of these normal mode states. The highly reactive $2\nu_1$ and $\nu_1 + \nu_3$ normal modes, being of A_1 and F_2 symmetry, can contribute to the $2\nu_3$-A_1 and $2\nu_3$-F_2 eigenstates, respectively, boosting their reactivity over the E component, which contains no ν_1 character due to symmetry. *Published by AIP Publishing.* [http://dx.doi.org/10.1063/1.4975025]

I. INTRODUCTION

The dissociative chemisorption of methane on transition metal surfaces has been studied in great detail both experimentally and by theoretical methods due to its importance in the steam reforming process used by the chemical industry to convert natural gas and water into synthesis gas.[1,2] Methane dissociation on Ni(111) occurs by a direct mechanism where the incident molecules either dissociate on impact to form CH_3(ads) + H(ads) or scatter non-reactively back into the gas phase. Early molecular beam experiments have shown that methane dissociation can be activated both by incident translational energy and vibrational excitation of the incident molecule.[3,4] Quantum state resolved reactivity measurements using laser preparation of different vibrational modes of the methane clearly show that the dissociation is mode specific[5] and bond selective.[6,7] Alignment of the incident methane molecules by polarized laser radiation uncovered steric effects in methane dissociation.[8,9] To date, state resolved reactivity data for the dissociation of CH_4 on Ni(111) and Ni(100) have been published[10–12] for the states $v = 0$, ν_3, ν_1, $\nu_2 + \nu_4$, $2\nu_3$-F_2, and $3\nu_4$.

We have recently introduced state preparation by double resonance excitation[13] for state resolved sticking coefficient measurements of CH_4 prepared in overtone and combination vibrations, including states that cannot be prepared by single photon excitation from the vibrational ground state due to symmetry restrictions. Here, we report the first results of state resolved reactivity measurements on Ni(111) for CH_4 prepared in the states $\nu_1 + \nu_3$, $2\nu_3$-F_2, $2\nu_3$-A_1, and $2\nu_3$-E. In Sec. II we briefly describe our experimental methods and in Sec. III we report our findings. Surprisingly, for these four eigenstates, as the vibrational energy increases the dissociative sticking probability decreases. In addition, the difference in reaction probability between the lowest energy and highest energy state can be quite large: roughly an order of magnitude. First, we examine this behavior using simple models that describe to what extent the vibrational amplitude for these states can localize on a single C–H stretch. We then compare the experimental data to the predictions of first principles quantum dynamical calculations, using a potential energy surface based on DFT (Density Functional Theory). The theory reproduces both the rough magnitude and overall reactivity trends observed in the experiments, and provides additional understanding of the origins of the observed behavior. We conclude with a brief summary in Sec. IV.

II. EXPERIMENTAL

The C–H stretching overtone vibrations of CH_4 include $2\nu_1$, $\nu_1 + \nu_3$, and $2\nu_3$, where $2\nu_1$ is the nondegenerate (A_1) overtone of ν_1, the symmetric C–H stretch normal mode, $\nu_1 + \nu_3$ the combination vibration of symmetric and antisymmetric C–H stretch, and $2\nu_3$ the overtone of the triply degenerate (F_2) antisymmetric C–H stretch normal mode ν_3. While the $2\nu_3$ overtone vibration is sixfold degenerate in the harmonic

approximation, it splits due to anharmonicity into three vibrational components with A_1, E, and F_2 symmetry in the T_d group. Of these, only the F_2 component is accessible by direct single photon overtone excitation from the v = 0 ground state of A_1 symmetry. However, using IR-IR double resonance excitation with two infrared photons, it is possible to prepare $CH_4(2\nu_3)$ in all three vibrational symmetry components[14,15] and compare the effect of these nearly isoenergetic vibrations on the dissociative chemisorption probabilities of CH_4 on a clean Ni(111) surface. A simplified level-diagram of the excitation path is shown in Figure 1.

The molecular beam/surface science apparatus, the state specific reactant preparation by rapid adiabatic passage (RAP), and the product detection by AES have been described in previous publications.[16,17] Briefly, a continuous molecular beam of methane was generated by expanding pure CH_4 or 3% CH_4 seeded in helium with a backing pressure of 2 bar through a temperature controlled nozzle of 30 μm diameter. A 1 mm diameter nickel skimmer was used to extract a molecular beam from the supersonic expansion. The speed distribution of the molecular beam for different seed ratios and nozzle temperatures was measured by time-of-flight techniques with an on-axis quadrupole mass-spectrometer (QMS) and a chopper-wheel. Table I shows the average kinetic energy $E_0 = 1/2mv_0^2$ and the translational temperature T_{trans} of CH_4 in the molecular beam obtained by fitting a flux weighted Maxwell Boltzmann speed distribution f(v) to the TOF data,

$$f(v) = v^3 \exp\left[\frac{m}{2kT_{trans}}(v - v_0)^2\right].$$

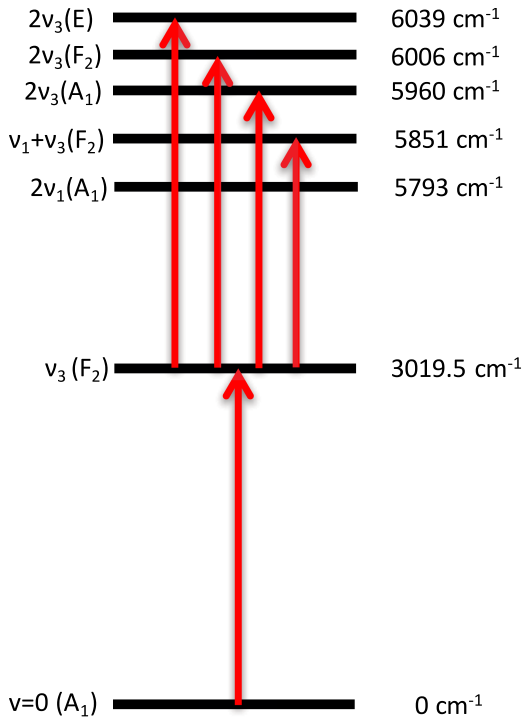

FIG. 1. Level diagram of the C–H stretch overtone states $\nu_1 + \nu_3$, $2\nu_3$-F_2, $2\nu_3$-A_1, and $2\nu_3$-E prepared by double resonance excitation. The excitation path for all four overtone states starts from v = 0, J = 1 using the ν_3 = 1, J = 0 level as intermediate state. The symmetric C–H stretch overtone $2\nu_1$ is included in the diagram but could not be prepared in this work.

TABLE I. Average kinetic energy E_0 and translational temperature T_{trans} of CH_4 for the molecular beam conditions used for the state-resolved sticking coefficient measurements.

CH_4 seed ratio (%)	T_N (K)	E_0 (kJ/mol)	T_{trans} (K)
100	305	9.3	20
3 in He	300	23	7
3 in He	473	37	23

Two independently tunable continuous wave infrared optical parametric oscillators (OPO-1 and OPO-2, Argos Acculight) were used for state specific preparation of overtone excited CH_4 by double resonance excitation. The OPO idler frequencies were stabilized by locking them to sequential rovibrational transitions ($v = 1 \leftarrow 0$ to $v = 2 \leftarrow 1$) of CH_4 using Doppler-free absorption features detected in static gas cells. OPO-1 was locked to a Lamb dip of the P(1) ν_3 fundamental transition of CH_4 at 3009.0114 cm^{-1} detected in the Doppler-broadened absorption line using a static gas cell at room temperature.[18] The 3.4 W idler output of OPO-1 traversed a second gas cell of 90 cm length filled with 150 μbar of CH_4 where it selectively pumps population from v = 0, J = 1 to ν_3 = 1, J = 0 only for molecules moving perpendicular to the IR beam. The Doppler-free population created by OPO-1 was probed by overlapping the pump and probe IR beams in the gas cell and scanning OPO-2 over the R(0), $\nu_3 = 2 \leftarrow 1$ transition. OPO-2 was then frequency locked to the peak of the Doppler-free absorption signal for R(0), $\nu_3 = 2 \leftarrow 1$ transition with a FWHM of 3.5 MHz.

The idler outputs of OPO-1 and OPO-2 were focused by cylindrical lenses (f = 25.4 cm) to intersect the molecular beam at two locations separated by 30 mm to excite CH_4 in an IR-IR double resonance scheme by rapid adiabatic passage 25 mm from the Ni(111) surface. Details of the RAP excitation have been described earlier.[16] A pyroelectric detector could be moved into the molecular beam past the excitation region to detect and quantify the flux of vibrationally excited molecules in order to verify that complete population inversion was achieved in both excitation steps.

III. RESULTS AND DISCUSSION

A. Experiment: State resolved reactivity measurements

State resolved reactive sticking coefficients of CH_4 prepared in four different C–H stretch overtone eigenstates were measured on the Ni(111) surface held at surface temperature T_s = 475 K. The nascent dissociation products of the incident CH_4 are a chemisorbed methyl group, CH_3(ads), and a hydrogen atom H(ads). At T_s = 475 K, CH_3(ads) rapidly dehydrogenates to form C(ads) and H(ads). The hydrogen atoms leave the Ni(111) surface by associative desorption to form H_2(g). Following a deposition experiment, the surface coverage of C(ads) was measured locally by Auger electron energy spectroscopy (AES) by scanning the sample surface in front of a commercial cylindrical mirror analyzer AES system (Omicron AES-150). Figure 2 shows a typical AES trace obtained by performing line scans across the 10 mm diameter Ni(111)

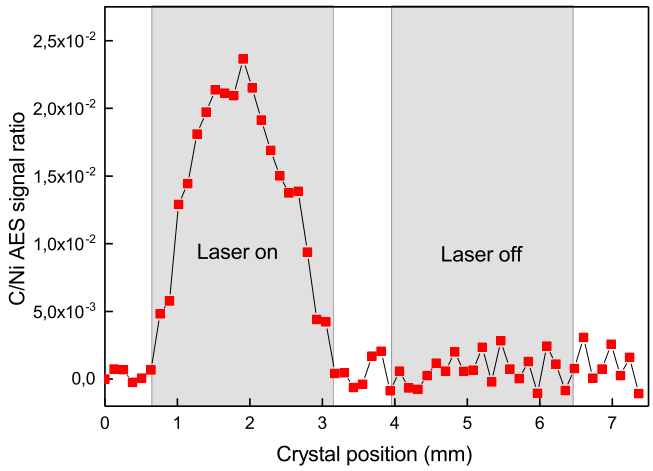

FIG. 2. AES analysis of chemisorbed carbon C(ads) formed by the dissociative chemisorption of CH_4 on the Ni(111) surface at T_s = 475 K.

single crystal surface. The molecular beam containing 3% CH_4 in He was deposited twice, at two different positions on the Ni(111) surface. The first deposition (Fig. 2 left, labeled "laser-on") was done with laser preparation of the $2\nu_3$-A_1 state of CH_4 and the second deposition (Fig. 2 right, labeled "laser off") without laser preparation leaving the incident CH_4 in the vibrational ground state (v = 0). Significant carbon deposition is detected only when the incident molecular beam contained vibrationally excited CH_4 demonstrating the strong enhancement of the dissociation probability due to overtone excitation. The incident dose of methane was monitored throughout each deposition experiment by a calibrated quadrupole mass spectrometer located in the UHV chamber. The incident flux of vibrationally excited methane was monitored before the start and at the end of each deposition by the pyroelectric detector.

Figure 3 shows the state resolved initial sticking coefficients S_0 obtained by AES analysis for the $\nu_1 + \nu_3$ state and the three $2\nu_3$ states of different vibrational symmetry as a function of incident translational energy E_t. The data for E_t = 9 and 23 kJ/mol show strong mode specificity where the state resolved reactivities appear to be inversely correlated with the

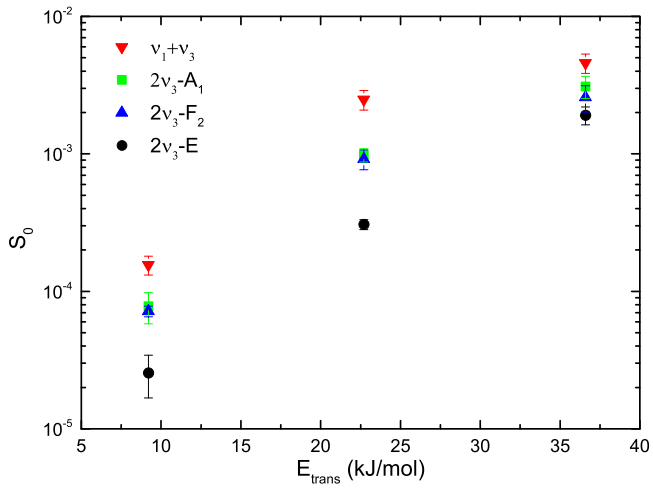

FIG. 3. State resolved initial dissociative sticking coefficients S_0 of CH_4 on Ni(111) for four different C–H overtone states (all J = 0) as functions of incident translational energy E_t and T_s = 475 K.

vibrational energy of the eigenstates. Preparation of CH_4 in the $\nu_1 + \nu_3$ eigenstate with the lowest vibrational energy of 5851 cm^{-1} results in nearly an order of magnitude higher reactivity than in the highest energy state $2\nu_3$-E state at 6054 cm^{-1}. $S_0(2\nu_3\text{-}A_1)$ and $S_0(2\nu_3\text{-}F_2)$ are the same within the experimental error and fall in between the reactivity range spanned by $S_0(\nu_1 + \nu_3)$ and $S_0(2\nu_3\text{-E})$. At the highest translational energy studied (37 kJ/mol), the difference between the state resolved reactivities decreases while the ordering stays the same.

The fact that the reactivity of the four different C–H stretch overtone states does not scale with their rovibrational energy excludes a prediction of the reaction rate by statistical theories.[19,20] Rather, the ordering of the CH_4 reactivity of the four overtone states may be rationalized by considering the differences in localization of the C–H stretch amplitudes for these states. Abram *et al.*[21] analyzed the C–H stretch overtone states of CH_4 using anharmonic symmetrized internal coordinates (SIC), expanding the vibrational states in a local mode basis. One can put 2 quanta of energy in a single C–H stretch 4 ways, denoted $|2000\rangle$, $|0200\rangle$, $|0020\rangle$, and $|0002\rangle$. The corresponding SIC states are orthonormal linear combinations of these states that transform like the irreducible representations of the T_d point group. We get one symmetric combination of A_1 symmetry and three antisymmetric combinations of F_2 symmetry, denoted $|2000;A_1\rangle$ and $|2000;F_2\rangle$, respectively. Similarly, there are 6 ways to put one quantum of energy each into two *different* C–H stretches; $|1100\rangle$, $|1010\rangle$, etc. These can be combined into 6 delocalized SIC modes of A_1, E, and F_2 symmetry, denoted $|1100;A_1\rangle$, and so on.[21] In Table II we list the percent contributions to the C–H stretch overtone states using this SIC basis set. We see that the C–H stretch amplitude is most strongly localized in a single C–H bond for the $\nu_1 + \nu_3$ eigenstate, followed by $2\nu_1$, then the $2\nu_3$-A_1 and $2\nu_3$-F_2-symmetry states, while for the $2\nu_3$-E symmetry state the C–H amplitude is completely delocalized and contains only $|1100\rangle$ character. The stronger localization of the C–H stretch amplitude in a single C–H bond for the vibrations of A_1- and F_2-symmetry is consistent with the higher reactivity of these states compared to the E-state with its delocalized vibrational amplitude. In addition, given the anharmonicity of the C–H stretch, the $|2000\rangle$ states are lower in energy than the $|1100\rangle$ states, and increased $|2000\rangle$ character results in a lower energy for the $2\nu_3$ states. The result is the observed anti-correlation between vibrational energy and reactivity for the three $2\nu_3$ overtone states.

This behavior is analogous to the mode specificity observed[5] for the dissociation of CH_2D_2 on Ni(100) where the $|2\rangle$ local mode state (two quanta of C–H stretch excitation localized in a single C–H bond) has been measured

TABLE II. Composition, as a percent, of the C–H stretch overtone states of CH_4, in the SIC local mode basis. Data taken from Ref. 21.

State	$\bar{\nu}$ (cm^{-1})	$\|2000;A_1\rangle$	$\|2000;F_2\rangle$	$\|1100;A_1\rangle$	$\|1100;E\rangle$	$\|1100;F_2\rangle$
$2\nu_3$-E	6039	···	···	···	100	···
$2\nu_3$-F_2	6006	···	11	···	···	88
$2\nu_3$-A_1	5960	44	···	56	···	···
$\nu_1 + \nu_3$	5851	···	88	···	···	11
$2\nu_1$	5793	56	···	44	···	···

to be as much as five times more reactive than the delocalized |11⟩ state (one quantum of C–H stretch in each of the two C–H bonds). DFT calculations[22] of the transition state (TS) structure for methane dissociation on Pt and Ni surfaces predict that the dissociating C–H bond is significantly stretched (r_{C-H} = 1.49 Å for the TS on Pt(111) compared to 1.09 Å for the gas phase). Localizing the C–H stretch amplitude in a single C–H bond via excitation of a state with |20⟩ character makes the reactant resemble the transition state more than excitation of a |11⟩ state which distributes the C–H amplitude over two C–H bonds, one of which becomes a spectator in the dissociation.[23] Jiang and Guo[24] expressed this idea of deforming the reactant towards the transition state structure in a quantitative way by proposing a sudden vector projection (SVP) model. The SVP model calculates the projection of the reactant vibrational state (vector) onto the transition state structure and establishes a correlation between the magnitude of the SVP value for a given vibrational state and the promotional effect of this state on the reactivity. Unfortunately, the SVP model cannot be applied to overtone states. In addition, as a sudden model, the SVP approach neglects intramolecular vibrational redistribution (IVR) that can occur during the approach of the reaction partners.

Even if the initial vibrational state does not already localize the C–H stretch amplitude in a favorable way for the reaction, surface induced IVR may still lead to such a localization and can therefore be responsible for vibrational mode specific reactivity in a gas/surface reaction. This is consistent with the experimentally observed[11,25] mode specificity between the ν_1 and the ν_3 mode of CH_4. Here, the four dimensional vibrationally adiabatic model described by Halonen *et al.*[26] predicts that the totally symmetric A_1 normal mode ν_1 evolves adiabatically to a localized excitation in a single C–H bond pointing towards the surface. On the other hand, the initially prepared antisymmetric F_2-ν_3 normal mode becomes localized on the CH_3 moiety pointing away from the surface. Based on this difference in C–H stretch localization, Halonen *et al.* predict that exciting the ν_1 mode will increase the dissociation probability more than the nearly isoenergetic ν_3 mode.

The SIC formulation provides a very satisfying picture, but it clearly has limitations. We see, for example, in Fig. 3 that the reactivities of the $2\nu_3$-A_1 and -F_2 states are about the same, while in Table II the A_1 component has 4 times the |2000⟩ character as the F_2 component. Also, as noted, molecules excited to the ν_1 state can be more reactive than those excited to the ν_3 state, even though the SIC representations of these two states differ only in the relative phases of the C–H vibrations. Another complication is that anharmonicity mixes the normal mode states. In Table III we show the results of a 4th order perturbative calculation by Wang and Sibert,[27] who computed the vibrational eigenstates of methane using a dressed normal mode basis set with an accurate *ab initio* quartic force field. From now on, to distinguish between the true vibrational eigenstates and their normal mode components, we will include the symmetry label when we refer to the eigenstate, as we have already done with $2\nu_3$-E, etc. Thus, in Table III, the $2\nu_1$-A_1 eigenstate is comprised of 74% of the $2\nu_1$ normal mode, 13% of the $2\nu_3$ normal mode, and so on. Note the bend character

TABLE III. Composition, as a percent, of the C–H stretch overtone states of CH_4, in terms of the normal mode basis set of Ref. 27.

State	$2\nu_3$	$\nu_1+\nu_3$	$2\nu_1$	$\nu_1+2\nu_2$	$\nu_2+\nu_3+\nu_4$	$\nu_3+2\nu_2$
$2\nu_3$-E	94	···	···	···	5	···
$2\nu_3$-F_2	73	15	···	···	4	6
$2\nu_3$-A_1	48	···	12	29	6	···
$\nu_1+\nu_3$-F_2	6	48	···	···	13	···
$2\nu_1$-A_1	13	···	74	3	3	···

of the eigenstates: ν_2 is the doubly degenerate bend and ν_4 is the triply degenerate bend. As the frequencies of the stretch modes are about twice that of the bending modes, the 2-quanta stretch states mix with 1-quantum stretch plus 2-quanta bend states such as $\nu_1+2\nu_2$ and $\nu_2+\nu_3+\nu_4$, and even some 4-quanta bend states (not shown). It is interesting to revisit our analysis based on the SIC states, given this mixing. For example, we can compute the percentage of |2000⟩ local mode character in the $2\nu_3$-F_2 state as 0.73(11%) + 0.15(88%) = 21%. Similarly, we find 0%, 28%, 43% and 47% |2000⟩ character for the $2\nu_3$-E, $2\nu_3$-A_1, $\nu_1+\nu_3$-F_2, and $2\nu_1$-A_1 states, respectively. This is a bit more consistent with experiment than the earlier analysis, as it now suggests that the F_2 and A_1 components of $2\nu_3$ have similar reactivities.

However, these reactions are clearly more complicated than can be explained by a model that includes only C–H stretching motions. Not only do bending types of motion contribute significantly to the states excited in the experiment, we see in Table III that the dissociative sticking probability actually *increase* as the amount of bending character increases. The excited state with the largest S_0 in our experiments, $\nu_1+\nu_3$-F_2, is comprised of only 54% 2-quanta stretch normal modes, with the next largest contribution (29%) coming from the 4-quanta bend[27] $3\nu_2+\nu_4$. Clearly, bending types of motion are very important as demonstrated by state resolved reactivity measurements for methane dissociation on Pt(110) where the vibrational efficacy of stretch-bend combination states was observed to be higher than for both pure stretch overtones and bend overtone states.[28]

B. Theory: Reaction path Hamiltonian (RPH) model for methane dissociation

Jackson and co-workers have developed a first-principles model for CH_4 dissociation based on a minimum energy reaction path calculated by DFT. We only briefly review this model here, as details can be found in several recent publications.[29–32] The DFT-based Vienna *ab initio* simulation package (VASP), developed at the Institut für Materialphysik of the Universität Wien,[33–37] is used to compute total energies. The interactions between the ionic cores and the electrons are described by fully nonlocal optimized projector augmented-wave (PAW) potentials,[37,38] and we use the Perdew-Burke-Ernzerhof (PBE) functional[39,40] to treat exchange-correlation effects. The Ni(111) surface is modeled as a series of infinite slabs separated by large vacuum space, using a 4-layer 3 × 3 supercell with periodic boundary conditions. To generate our full-dimensional potential energy surface we first locate the minimum energy path (MEP) for reaction, and compute the total energy $V_0(s)$

at several dozen points along this path. The distance along the path in mass-weighted coordinates is s. At each of these points, we compute and diagonalize the force-projected Hessian to find the 14 normal vibrational coordinates Q_k and corresponding frequencies $\omega_k(s)$ describing motion orthogonal to the reaction path in the harmonic approximation. Ignoring any higher order anharmonic terms, our potential can be written as follows:

$$V = V_0(s) + \sum_{k=1}^{14} \frac{1}{2}\omega_k^2(s) Q_k^2. \quad (1)$$

In Fig. 4, we plot $\hbar\omega_q(s)$ along the reaction path for CH_4 chemisorption on Ni(111). When methane is far above the surface there are nine bending and stretching normal modes with nonzero frequency. The remaining five modes correspond to rotational and translational motion at large negative s. At the transition state (s = 0), the carbon atom is roughly over the top site and the reacting C–H bond is angled towards the metal, with the other three C–H bonds angled away. The MEP is symmetric with respect to reflection through a plane perpendicular to the surface and including the reacting bond. We label the 9 normal modes comprising the bends and stretches as 1′–6′ and 1″–3″ to indicate whether they are symmetric (A′) or antisymmetric (A″) with respect to this reflection.

We write the total molecular wave function as follows:

$$\Psi(t) = \sum_{\mathbf{n}} \chi_{\mathbf{n}}(s;t) \prod_k \phi_{n_k}(Q_k;s), \quad (2)$$

where the ϕ_{n_k} are harmonic oscillator eigenfunctions that depend parametrically on s, because $\omega_k(s)$ varies along the reaction path. The corresponding eigenvalues are $\hbar\omega_k(s)\left(n_k + \frac{1}{2}\right)$, and the vector **n** labels the vibrational state corresponding to the set of quantum numbers $\{n_k\}$. The coupled equations of motion for the wave packets, $\chi_{\mathbf{n}}(s;t)$, are of the form[30]

$$i\hbar\frac{\partial\chi_{\mathbf{n}}(s;t)}{\partial t} = \left[\frac{1}{2}p_s^2 + V_0(s) + \sum_{k=1}^{14}\hbar\omega_k(s)\left(n_k + \frac{1}{2}\right)\right]\chi_{\mathbf{n}}(s;t) + \sum_{\mathbf{n}'} F_{\mathbf{n}\mathbf{n}'}\chi_{\mathbf{n}'}(s;t). \quad (3)$$

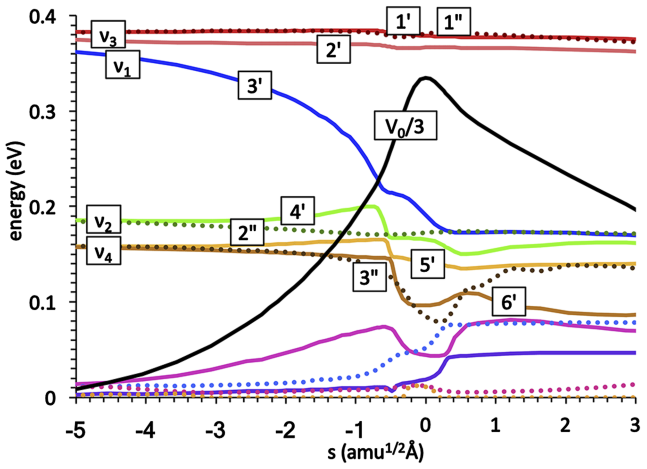

FIG. 4. Total energy, $V_0(s)$, rescaled by 1/3, and energies of the normal vibrational modes, $\hbar\omega_q(s)$, along the reaction path for the dissociative chemisorption of CH_4 on Ni(111).

The wave packets thus evolve on vibrationally adiabatic potential energy surfaces corresponding to each vibrational state **n**, and the operators $F_{\mathbf{n}\mathbf{n}'}$ couple states of the same symmetry (A′ or A″). The $F_{\mathbf{n}\mathbf{n}'}$ are proportional to the vibrationally nonadiabatic couplings, computed using the eigenvectors from the diagonalization of the Hessians along the reaction path.

The sums over **n** in Eqs. (2) and (3) include the vibrationally adiabatic ground state and all states with one or two vibrational quanta excited. Detailed expressions for the equations of motion and the coupling terms can be found in a recent publication.[41] For a given initial vibrational state, $\mathbf{n_0}$, standard techniques are used to evolve the wave packets and to energy-analyze the reactive flux.[30,31] The result is the rigid-lattice reaction probability, $P_0(E_t, \mathbf{n_0})$. The five normal modes that have small frequencies when the molecule is far above the surface describe molecular translation parallel to the surface and rotation away from the MEP. Unlike the internal stretch and bend vibrations included in the $\Phi_{\mathbf{n}}$, these other types of motion are not well described by a harmonic model, and must be treated differently. These five modes do not couple strongly to the internal bends and stretches in the entrance channel. The location of the molecular center of mass over the unit cell, X and Y, changes little along the MEP in the entrance channel, with the carbon atom remaining more-or-less over the minimum barrier site. The rotation of the molecule in the entrance channel also follows the MEP. Thus, P_0 corresponds to reaction at the minimum barrier site only, with rotational motion treated adiabatically.

To compute the dissociative sticking probability S_0, we average P_0 over all other surface impact sites, correct the rotational treatment, and include the effects of lattice motion. At the relatively low collision energies of the experiment, reaction is only possible close to the MEP, and we use the following approximation to average over paths corresponding to impacts near the lowest barrier sites. Motion along X and Y is slow on collision time scales, given the relatively large molecular mass and our normal incidence conditions. Assuming that there is no steering of the incident methane along X and Y, we average P_0 over all impact sites in the surface unit cell, using the following approximation to estimate P_0 for impact at a site (X, Y) away from the minimum barrier site:

$$P_0(E_i, \mathbf{n_0}; X, Y) \approx P_0(E_i - \Delta V, \mathbf{n_0}). \quad (4)$$

$\Delta V(X, Y)$ is the increase in barrier height at (X, Y) relative to the minimum barrier site, which we can approximate using the normal modes, or compute directly using DFT. Recent AIMD studies confirm this sudden behavior for X and Y.[42,43] These same studies suggest that the rotational behavior might be closer to sudden at high collision energies,[42,43] while it should be closer to adiabatic at lower incident energies. We use an approach similar to Eq. (4) to estimate S_0 in the sudden limit,[42] and define our final S_0 as a linear combination of these two limits, such that the behavior is adiabatic at lower incident energies and sudden at higher incident energies.[29] Finally, to introduce the effects of lattice motion for a surface temperature T, we average P_0 over all displacements and momenta normal to the surface of the Ni atom over which methane dissociates.[44,45] The momentum of this atom determines the relative collision velocity, and the displacements can

significantly change the barrier height. We use a Debye model to describe the motion of this Ni atom.[29]

In Fig. 5 we plot the computed dissociative sticking probabilities S_0 for the ground and several excited states of CH_4. Note that these are the harmonic normal mode eigenstates. For the ground state, we show both the rotationally sudden and adiabatic limits. The difference is roughly a factor of 4 in the sticking. For the excited states, we find that $S_0(E_t,\nu_1) > S_0(E_t,\nu_3)$. While this behavior has been observed experimentally on Ni(100)[11,25] and reproduced by our RPH-based model,[30] no data exist for $S_0(E_t,\nu_1)$ on Ni(111). As noted, the vibrationally adiabatic model of Halonen *et al.* predicts that as CH_4 moves towards the surface the vibrational motion becomes localized on the reacting C–H stretch for molecules excited to the ν_1 state, while for molecules in the ν_3 state it localizes on the non-reacting methyl group.[26] Thus, molecules excited to the ν_1 state are likely to be more reactive. We see the same behavior in our model, corresponding to the strong mode softening of the $\nu_1 = 3'$ mode in Fig. 4. As the molecule approaches the transition state, the reacting C–H bond weakens, its frequency decreases, and it decouples from the relatively unperturbed higher-frequency C–H stretches in the non-reacting methyl group. This is the origin of the vibrational localization observed in the model of Halonen *et al.* However, our model also includes the non-adiabatic coupling between these states, and this turns out to be extremely important. In the adiabatic limit ($F_{nn'} = 0$ in Eq. (3)) each wave packet remains on the vibrationally adiabatic potential energy surface corresponding to its vibrational state. Because of mode softening, the barrier along the vibrationally adiabatic reaction path for the ν_1 state is lowered to 0.70 eV, while for the ν_3 state it is about 0.87 eV (an average of the 1′, 2′ and 1″ components), similar to the vibrational ground state. While the barrier for reaction is significantly lower along the ν_1 adiabatic path, this only partly explains the mode specificity, as much of the data in Fig. 5 are for energies below these barriers. At these low energies, the mechanism for reaction involves vibrationally non-adiabatic transitions between states, though lattice motion effects can also be very important. For example, a molecule initially in the 3′ state can jump to the 4′ state at the avoided crossing, and then to the 5′ state, and so on. As the wave packet transitions to vibrational states of lower energy, the excess energy is converted to motion along the reaction path, increasing the reaction probability. In addition, the modes exchange character at the crossings, preserving the localization of vibrational energy on the reactive C–H bond. We find a strong non-adiabatic coupling at all the avoided crossings of Fig. 3,[29] as well as between the 2′ and 3′ modes far above the surface where they are nearly degenerate (peaking near s = −5). This surface induced IVR is responsible for much of the behavior observed in the experiments. Molecules excited to either the 2′ or 3′ mode exhibit similar behavior, as these modes mix in the entrance channel. The 1′ mode couples only weakly to the 2′ or 3′, and the 1" does not couple to the A′ modes at all due to symmetry. Thus, we predict that Ni(111) molecules in the ν_1 (3′) state are two to three times more reactive than molecules in the ν_3 (1′, 2′, 1″) state. Note that a purely vibrationally adiabatic model predicts that molecules in the ν_3 state are about as reactive as those in the ground state. In fact, experiment, like our theory, finds a strong vibrational enhancement;[25,46,47] the ν_1 enhancement is simply larger.

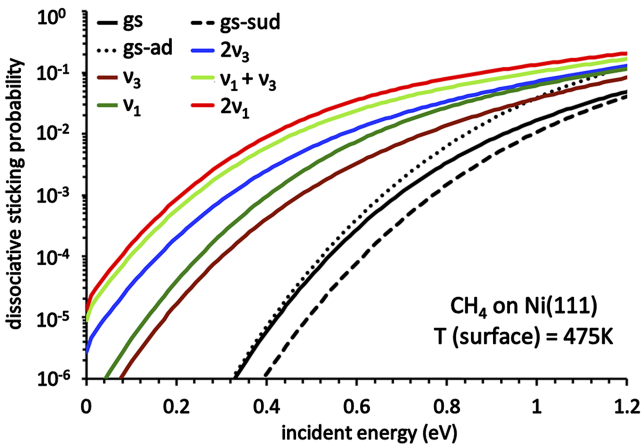

FIG. 5. Dissociative sticking probability of CH_4 on Ni(111) vs incident energy E_t, for the molecule in the ground state (gs) or vibrationally excited (normal mode) states indicated. Results for both the rotationally adiabatic and sudden limits are also plotted for the ground state.

These same ideas explain the behavior of the two-quanta stretch overtones. Due to the 3′ mode softening the (average) vibrationally adiabatic barriers for the $2\nu_1$, $\nu_1 + \nu_3$, and $2\nu_3$ states are 0.52, 0.69, and 0.86 eV, respectively. We see in Fig. 5 that sticking follows this trend, $S_0(E_t, 2\nu_1) > S_0(E_t, \nu_1 + \nu_3) > S_0(E_t, 2\nu_3)$, and mode softening certainly contributes to this behavior at higher energies. At energies below these barrier heights, however, lattice motion and non-adiabatic transitions are responsible for reaction. The preferred reaction path is 3′ to 4′ to 5′ and so on, and the $2\nu_1$ (=3′ + 3′) state is thus the most reactive, followed by $\nu_1 + \nu_3$. The components of $\nu_1 + \nu_3$ and $2\nu_3$ that contain 2′, such as 3′ + 2′ and 2′ + ′2, respectively, are more reactive than those containing 1′ and 1″, because surface induced IVR mixes 2′ with 3′.

This is also consistent with much of the experimental data in Fig. 3. We see that molecules in the $\nu_1 + \nu_3$ state are more reactive than those in one of the $2\nu_3$ components. In addition, looking at Table III, the most reactive symmetry components of $2\nu_3$ are those containing $2\nu_1$ and $\nu_1 + \nu_3$ character. However, we can take this a bit further by actually propagating the true (mixed) eigenstates computed by Wang and Sibert[27] (see Table III). Using our reaction path approach, it is possible to write an initial state of the form $c_a\,|\nu_a\rangle + c_b\,|\nu_b\rangle$, where $|\nu_a\rangle$ and $|\nu_b\rangle$ are two harmonic normal modes, propagate the total wave function, and compute S_0. However, we have found that this gives the same result as simply averaging the normal mode sticking probabilities; i.e., $c_a^2\,S_0\,(\nu_a) + c_b^2\,S_0\,(\nu_b)$. We take the latter approach here.

A minor problem is that we are not able to directly calculate sticking probabilities for initial vibrational states that contain three or more quanta, and these contribute to some of the eigenstates excited in the experiments (see Table III). However, we can reasonably estimate S_0 for these states by examining how the S_0 vs. E_t curves shift with vibrational excitation. In Fig. 6 we see that the computed S_0 curve for the ν_2 state is shifted about 0.11 eV from the S_0 curve for the ground state. The curve shifts about 0.10 eV from the ν_2 state to the $2\nu_2$ state, which is slightly smaller as the total molecular energy

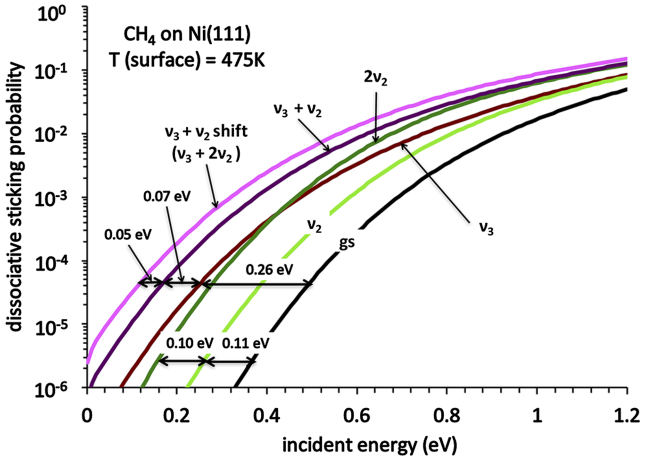

FIG. 6. The sticking probability for the $\nu_3 + 2\nu_2$ normal mode state estimated from single- and two-quanta states by shifting the curves.

is getting closer to the barrier height. If we add a quantum of ν_2 bend to the higher energy ν_3 state, we thus expect to see an even smaller shift, and indeed the S_0 curve shifts about 0.07 eV from the ν_3 state to the $\nu_3 + \nu_2$ state. Adding a quantum of ν_2 bend to an even higher energy state should lead to an even smaller shift, and we estimate that the S_0 curve is likely to shift about 0.05 eV from the $\nu_3 + \nu_2$ state to the $\nu_3 + 2\nu_2$, giving the curve in Fig. 6. Although this approach is arbitrary, the errors in the estimated energy shifts are likely to be small. In addition, as we will show, the overall reactivity is dominated by contributions from the $2\nu_3$, $\nu_1 + \nu_3$, and $2\nu_1$ normal mode components.

In Fig. 7 we plot the results of our calculations and compare with the experimental data from Fig. 3. Overall, the calculations reproduce the experimental trends, if not always the magnitude of the sticking. $2\nu_3$-E is the least reactive symmetry component, giving approximately the same S_0 as the normal mode $2\nu_3$ state, as it comprised almost entirely of this state (94%). The $2\nu_3$-A_1 and $2\nu_3$-F_2 symmetry components have contributions from the more reactive $2\nu_1$ and $\nu_3 + \nu_1$ normal mode states, making them more reactive than the $2\nu_3$-E

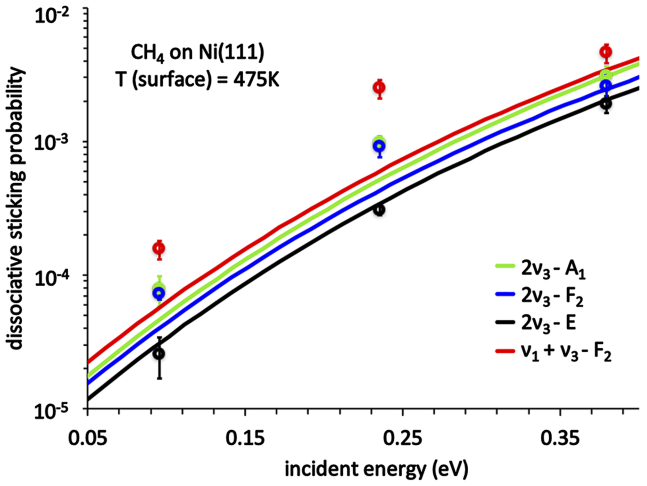

FIG. 7. Sticking probabilities for the $\nu_1 + \nu_3$-F_2 state and the different symmetry components of the $2\nu_3$ state. The lines are from the theory and the experimental data are from Fig. 3.

state, with $S_0(2\nu_3\text{-}A_1)$ a bit larger than $S_0(2\nu_3\text{-}F_2)$ in both theory and experiment. The $\nu_1 + \nu_3$-F_2 state is more reactive than any component of the $2\nu_3$ state, for the reasons discussed, but the difference is smaller than that observed in the experiments. At the highest energy of the experiments the theory reproduces both the ordering and the magnitude of the measured sticking probabilities quite well. At the lowest energy, the computed S_0 is too small by almost a factor of two for the $2\nu_3$-A_1 and $2\nu_3$-F_2 symmetry components and almost a factor of three for the $\nu_1 + \nu_3$ state. Thus, for these three states the experimentally measured efficacies for promoting a reaction become bigger, relative to that for the $2\nu_3$-E state, as the incident energy becomes very small. We note that similar behavior was found for the $2\nu_3$ symmetry states of CH_4 for dissociation on Ni(111). Our RPH-based calculation does not reproduce this change in the *relative* efficacy with energy, and the theory curves in Fig. 7 maintain roughly the same spacing at all energies considered. The origin of this behavior is not clear, though at these low energies the sticking probabilities can be very sensitive to the presence of defects. It is possible that the vibrational efficacies could be different on, say, step edges, than on the terrace sites.

Finally, it is interesting to note that the bend-plus-stretch combinations of Fig. 6 are reasonably efficacious for promoting dissociation. We find that, for example, at $E_t = 0.1$ eV, S_0 for the 1-stretch plus 2-bend combinations ($\nu_3 + 2\nu_4$, $\nu_2 + \nu_3 + \nu_4$, etc.) are all about the same, and only slightly smaller than $S_0(2\nu_3)$. However, at this energy, $S_0(\nu_1 + \nu_3)$ is three times larger and $S_0(2\nu_1)$ is almost five times larger. As a result the $2\nu_3$, $\nu_1 + \nu_3$, and $2\nu_1$ normal mode components dominate the overall reactivity of the states excited in the experiment. In the end, symmetry and the unique reactivity of the 3′ mode control the ordering in Fig. 3. Due to the latter, $S_0(2\nu_1) > S_0(\nu_1 + \nu_3) > S_0(2\nu_3)$. The $2\nu_1$ and $\nu_1 + \nu_3$ normal modes, being of A_1 and F_2 symmetry, can contribute to the $2\nu_3$-A_1 and $2\nu_3$-F_2 eigenstates, respectively, boosting their reactivity over the E component, which contains no ν_1 character due to its symmetry.

IV. SUMMARY

In summary, we have measured the state resolved dissociation probability of CH_4 on Ni(111) at T_s = 475 K for four different C–H stretch overtone states using double resonance excitation of the reactants and Auger detection of dissociation products. We propose that the observed mode specificity is due to differences in the degree of C–H stretch amplitude localization at the transition state for the different initially prepared states. We compare the state-resolved reactivity data obtained from our experiments with the results of quantum scattering calculations using a DFT-based potential energy surface. These calculations show that of all the normal vibrational modes of CH_4, the symmetric stretch, ν_1, has the largest efficacy for promoting a reaction. This is a result of the weakening of the reacting C–H bond as the molecule approaches the transition state. The corresponding drop in vibrational frequency causes this C–H stretch to decouple from the three nonreacting C–H stretches. Thus, as the molecule approaches the surface, one of the 4 C–H stretch normal modes will decrease in

frequency, and the vibrational amplitude will become localized on the reacting C–H bond. This particular mode adiabatically correlates with the ν_1 stretch, making molecules excited to this state unusually reactive. Vibrationally nonadiabatic transitions to lower states preserve this behavior and allow for reactions at energies below the vibrationally adiabatic barrier height. For these reasons, we find that overtone states with more ν_1 character are more reactive, and $S_0(2\nu_1) > S_0(\nu_1 + \nu_3) > S_0(2\nu_3)$. The $2\nu_3$ eigenstates excited in the experiment are split into three symmetry components due to anharmonicity, and each component contains contributions from these normal mode states, as well as various stretch plus two-bend normal mode states. The highly reactive $2\nu_1$ and $\nu_1 + \nu_3$ normal modes, being of A_1 and F_2 symmetry, can contribute to the $2\nu_3$-A_1 and $2\nu_3$-F_2 eigenstates, respectively, boosting their reactivity over the E component, which contains no ν_1 character due to its symmetry.

ACKNOWLEDGMENTS

We gratefully acknowledge financial support provided by the Swiss National Science Foundation (Grant No. 134709/1) and the Ecole Polytechnique Fédérale de Lausanne. B. Jackson gratefully acknowledges support from the Division of Chemical Sciences, Office of Basic Energy Sciences, Office of Energy Research, U.S. Department of Energy, under Grant No. DE-FG02-87ER13744. The authors would also like to thank Xiao-Gang Wang and Edwin L. Sibert III for providing data from their study of Ref. 27.

[1] J. H. Larsen and I. Chorkendorff, Surf. Sci. Rep. **35**, 163 (1999).
[2] F. Besenbacher, I. Chorkendorff, B. S. Clausen, B. Hammer, A. M. Molenbroek, J. K. Norskov, and I. Stensgaard, Science **279**, 1913 (1998).
[3] C. T. Rettner, H. E. Pfnür, and D. J. Auerbach, Phys. Rev. Lett. **54**, 2716 (1985).
[4] C. T. Rettner, H. E. Pfnür, and D. J. Auerbach, J. Chem. Phys. **84**, 4163 (1985).
[5] R. D. Beck, P. Maroni, D. C. Papageorgopoulos, T. T. Dang, M. P. Schmid, and T. R. Rizzo, Science **302**, 98 (2003).
[6] D. R. Killelea, V. L. Campbell, N. S. Shumann, and A. L. Utz, Science **319**, 790 (2008).
[7] L. Chen, H. Ueta, R. Bisson, and R. D. Beck, Faraday Discuss. **157**, 285 (2012).
[8] B. L. Yoder, R. Bisson, and R. D. Beck, Science **329**, 553 (2010).
[9] B. L. Yoder, R. Bisson, P. M. Hundt, and R. D. Beck, J. Chem. Phys. **135**, 224703 (2011).
[10] L. B. F. Juurlink, D. R. Killelea, and A. L. Utz, Prog. Surf. Sci. **84**, 69 (2009).
[11] P. Maroni, D. C. Papageorgopoulos, M. Sacchi, T. T. Dang, R. D. Beck, and T. R. Rizzo, Phys. Rev. Lett. **94**, 246104 (2005).
[12] H. Chadwick and R. D. Beck, Chem. Soc. Rev. **45**, 3576 (2016).
[13] P. M. Hundt, M. E. van Reijzen, H. Ueta, and R. D. Beck, J. Phys. Chem. Lett. **5**, 1963 (2014).
[14] A. Demartino, R. Frey, and F. Pradere, Chem. Phys. Lett. **100**, 329 (1983).
[15] A. Demartino, R. Frey, and F. Pradere, Chem. Phys. Lett. **95**, 200 (1983).
[16] H. Chadwick, P. M. Hundt, M. E. van Reijzen, B. L. Yoder, and R. D. Beck, J. Chem. Phys. **140**, 034321 (2014).
[17] M. P. Schmid, P. Maroni, R. D. Beck, and T. R. Rizzo, Rev. Sci. Instrum. **74**, 4110 (2003).
[18] W. Demtröder, *Atoms, Molecules and Photons: An Introduction to Atomic-, Molecular- and Quantum-Physics* (Springer, 2010).
[19] H. L. Abbott, A. Bukoski, and I. Harrison, J. Chem. Phys. **121**, 3792 (2004).
[20] H. L. Abbott, A. Bukoski, D. F. Kavulak, and I. Harrison, J. Chem. Phys. **119**, 6407 (2003).
[21] I. Abram, A. Demartino, and R. Frey, J. Chem. Phys. **76**, 5727 (1982).
[22] S. Nave, A. K. Tiwari, and B. Jackson, J. Chem. Phys. **132**, 054705 (2010).
[23] H. A. Bechtel, Z. H. Kim, J. P. Camden, and R. N. Zare, J. Chem. Phys. **120**, 791 (2004).
[24] B. Jiang and H. Guo, J. Phys. Chem. C **117**, 16127 (2013).
[25] L. B. F. Juurlink, P. R. McCabe, R. R. Smith, C. L. DiCologero, and A. L. Utz, Phys. Rev. Lett. **83**, 868 (1999).
[26] L. Halonen, S. L. Bernasek, and D. J. Nesbitt, J. Chem. Phys. **115**, 5611 (2001).
[27] X. G. Wang and E. L. Sibert, J. Chem. Phys. **111**, 4510 (1999).
[28] R. Bisson, M. Sacchi, and R. D. Beck, Phys. Rev. B **82**, 121404(R) (2010).
[29] H. Guo and B. Jackson, J. Chem. Phys. **144**, 184709 (2016).
[30] B. Jackson and S. Nave, J. Chem. Phys. **135**, 114701 (2011).
[31] B. Jackson and S. Nave, J. Chem. Phys. **138**, 174705 (2013).
[32] S. Nave, A. K. Tiwari, and B. Jackson, J. Phys. Chem. A **118**, 9615 (2014).
[33] G. Kresse and J. Hafner, Phys. Rev. B **47**, 558 (1993).
[34] G. Kresse and J. Hafner, Phys. Rev. B **49**, 14251 (1994).
[35] G. Kresse and J. Furthmuller, Phys. Rev. B **54**, 11169 (1996).
[36] G. Kresse and J. Furthmuller, Comput. Mater. Sci. **6**, 15 (1996).
[37] G. Kresse and D. Joubert, Phys. Rev. B **59**, 1758 (1999).
[38] P. E. Blochl, Phys. Rev. B **50**, 17953 (1994).
[39] J. P. Perdew, K. Burke, and M. Ernzerhof, Phys. Rev. Lett. **78**, 1396 (1997).
[40] J. P. Perdew, K. Burke, and M. Ernzerhof, Phys. Rev. Lett. **77**, 3865 (1996).
[41] A. Farjamnia and B. Jackson, J. Chem. Phys. **142**, 234705 (2015).
[42] B. Jackson, F. Nattino, and G. J. Kroes, J. Chem. Phys. **141**, 054102 (2014).
[43] F. Nattino, H. Ueta, H. Chadwick, M. E. van Reijzen, R. D. Beck, B. Jackson, M. C. van Hemert, and G. J. Kroes, J. Phys. Chem. Lett. **5**, 1294 (2014).
[44] A. K. Tiwari, S. Nave, and B. Jackson, Phys. Rev. Lett. **103**, 253201 (2009).
[45] A. K. Tiwari, S. Nave, and B. Jackson, J. Chem. Phys. **132**, 134702 (2010).
[46] R. R. Smith, D. R. Killelea, D. F. DelSesto, and A. L. Utz, Science **304**, 992 (2004).
[47] V. L. Campbell, N. Chen, H. Guo, B. Jackson, and A. L. Utz, J. Phys. Chem. A **119**, 12434 (2015).